Available online at www.sciencedirect.com

ScienceDirect

Advances in Space Research 52 (2013) 1545–1560

ADVANCES IN SPACE RESEARCH (a COSPAR publication)

www.elsevier.com/locate/asr

Long-term dynamics of high area-to-mass ratio objects in high-Earth orbit

Aaron J. Rosengren *, Daniel J. Scheeres

Department of Aerospace Engineering Sciences, University of Colorado at Boulder, Boulder, CO 80309, USA

Received 19 February 2013; received in revised form 23 July 2013; accepted 24 July 2013
Available online 1 August 2013

Abstract

The dynamics of high area-to-mass ratio (HAMR) objects has been studied extensively since the discovery of this debris population in near GEO orbits. A sound understanding of their nature, orbital evolution, and possible origin is critical for space situational awareness. In this paper, a new averaged formulation of HAMR object orbit evolution that accounts for solar radiation pressure, Earth oblateness, and lunisolar perturbations is explored. The first-order averaged model, explicitly given in terms of the Milankovitch orbital elements, is several hundred times faster to numerically integrate than the non-averaged counterpart, and provides a very accurate description of the long-term behavior. This model is derived and presented along with comparisons with explicit long-term numerical integrations of HAMR objects in GEO. The dynamical configuration of the Earth–Moon–Sun system was found to have a significant resonance effect with HAMR objects leading to complex evolutionary behavior. The properties of this resonant population may serve as important constraints for models of HAMR debris origin and evolution. A systematic structure associated with their distribution in inclination and ascending node phase space is identified. Given that these objects are difficult to target and correlate, this has many implications for the space surveillance community and will allow observers to implement better search strategies for this class of debris.

Keywords: High area-to-mass ratio objects; Space debris; Long-term dynamical evolution; Averaging; Orbit perturbations; Milankovitch orbital elements

1. Introduction

The motion of high area-to-mass ratio (HAMR) objects in high-Earth orbits has been studied extensively since the discovery of this debris by Schildknecht and colleagues (ca. 2004). The HAMR debris population is thought to have origins in the geostationary (GEO) region, and many of these objects are uncharacterized with apparent area-to-mass ratios of up to 30 meters squared per kilogram (Schildknecht et al., 2004; Liou and Weaver, 2005; Schildknecht, 2007). The orbits of HAMR objects are highly perturbed from the combined effect of solar radiation pressure (SRP), anomalies of the Earth gravitational field, and third-body gravitational interactions induced by the Sun and the Moon (Chao, 2006; Valk et al., 2008; Anselmo and Pardini, 2010; Scheeres et al., 2011; Rosengren and Scheeres, 2011). The evolution of individual orbits of HAMR debris over a considerable time interval, taking into account both short-period and long-period terms, can be calculated by numerical integration of the precise set of differential equations. This process leads to the construction of high-precision ephemerides and the investigation of the empirical evolution of such objects, but not necessarily to general insight into the dynamics of the problem. Numerical computations of this type have revealed that the amplitudes of the short-term fluctuations in the osculating orbital elements are, in general, quite small when compared with the long-term variations. For this

* Corresponding author. Address: 431 UCB ECEE 166, Boulder, CO 80309-0431, USA. Tel.: +1 303 492 7826.
E-mail addresses: aaron.rosengren@colorado.edu (A.J. Rosengren), scheeres@colorado.edu (D.J. Scheeres).

0273-1177/$36.00 © 2013 COSPAR. Published by Elsevier Ltd. All rights reserved.
http://dx.doi.org/10.1016/j.asr.2013.07.033

reason, and the necessity of considering the orbital behavior of a large population of HAMR debris over many thousands of revolutions, it seems reasonable to investigate the equations that govern the long-term evolution of orbits. Such equations can be derived by the theory of secular perturbation.

The theory of secular perturbation, also referred to as the theory of averaging, was introduced by Clairaut, Lagrange, and Laplace over two centuries ago. In the classical Laplace–Lagrange theory, as in that of Gauss, Delaunay, Halphen, Poincaré-Lindstedt, von Zeipel, Brouwer, and the Lie-transformation of Hori and Deprit, the goal is to eliminate the short-period perturbation terms and derive the equations that capture the secular evolution of the system (Sanders et al., 2007). When the equations of motion do not have a canonical form, short-period terms can be eliminated systematically by means of the of the Krylov–Bogoliubov–Mitropolski method of averaging. This method, developed by Kyrloff and Bogoliuboff (1947) in the analysis of nonlinear oscillations, and generalized by Bogoliubov and Mitropolski (1961), was first applied to problems in celestial mechanics and satellite theory in the early 1960s (Musen, 1960; Musen, 1961; Struble, 1961; Allan, 1962; Lidov, 1962). Application of this method to astronomical problems provides a direct means of obtaining the first-order secular equations, and leads to equation which do not depend on expansions in either eccentricity or inclination. The averaged equations can be numerically integrated, with significantly reduced computational requirements, and often reveal the essential characteristics of the exact solution in a more satisfactory way than a numerical solution of the non-averaged equations.

Liou and Weaver (2005) used PROP3D, a fast orbit propagator based on the averaging principle that was developed for NASA's debris evolutionary models, to investigate the HAMR debris problem. PROP3D accounts for the perturbations from Earth gravity up to the fourth zonal harmonic, low-order lunisolar gravitational interactions, and SRP with consideration of the Earth shadow effect. Through comparisons with a high-fidelity orbit integrator, they showed that HAMR objects in GEO are dominated by major perturbations, not those of higher order. Chao (2006) performed long-term studies of the orbital evolution of GEO objects with high area-to-mass ratios through analytically averaged equations. Chao investigated the secular effects of SRP on the eccentricity and argument of perigee by averaging over the object's orbital period. The long-term motion of the orbit inclination and longitude of the ascending node were studied though doubly-averaged equations for the lunisolar attraction, ignoring higher-order terms in eccentricity, and singly-averaged equations for the SRP perturbation. The secular equations of motion were written in terms of the classical orbital elements, which leads to the presence of small numerical divisors–the eccentricity and the sine of the inclination.

We present a non-singular model of first-order averaging, explicitly given in terms of the Milankovitch vectorial elements, which accounts for solar radiation pressure, the oblateness of the Earth's gravitational figure, and lunisolar perturbations. The secular equations hold rigorously for all Keplerian orbits with nonzero angular momentum; they are free of the singularities associated with zero eccentricity and vanishing line of nodes. This paper is organized into the following discussions. We first present the environment and force models for each perturbation, and discuss any underlying assumptions and approximations. We then review the Milankovitch elements and give their perturbation equations in Lagrangian form, assuming the perturbing accelerations are expressible as gradients of a disturbing function. After deriving the first-order averaged equations for each perturbing force, we demonstrate their validity by comparing numerical integrations of them to integrations of the exact Newtonian equations. The extent to which the qualitative properties of the orbit persist with increasing area-to-mass is investigated. We then show how the geometry of the Earth–Moon–Sun system, and in particular the regression of the lunar node, causes a resonance effect with a particular class of HAMR objects, leading to complex evolutionary behavior. The properties of this resonant population may serve as important constraints for models of HAMR debris origin and evolution. We then launch a range of HAMR objects, released in geostationary orbit (equatorial, circular-synchronous) with area-to-mass ratios from 0 up to 40 m^2/kg, uniformly distributed in lunar node, and predict the spatial distribution of the population. We identify a systematic structure associated with their distribution in inclination and ascending node phase space, which is similar to that of the uncontrolled GEO satellites. Finally, we discuss the implications of these results for observing campaigns and our future research directions.

2. Environment and force models

2.1. The Earth–Moon–Sun system

Any account of motion in the Earth–Moon–Sun systems has to start with a description of the dynamical configuration of this three-body problem. Perozzi et al. (1991), using eclipse records, the JPL ephemeris, and results from numerical integration of the three-body problem, showed that the mean geometry of the Earth–Moon–Sun system repeats itself closely after a period of time equal in length to the classical eclipse prediction cycle known as the Saros. That is, this dynamical system is moving in a nearly periodic orbit. Saros means repetition, and indicates a period of 223 synodic months ($\sim$ 6585.3213 days), after which the Sun has returned to the same place it occupied with respect to the nodes of the Moon's orbit when the cycle began. While the motion of the Earth around the Sun can, over time spans of interest, be considered Keplerian, the Moon is incessantly subject to solar perturbations

resulting in periodic and secular variations of its orbital elements (Roy, 2005). The semi-major axis, eccentricity, and inclination are subject to periodic variations about their mean values of 384,400 km, 0.0549, and 5°09′, respectively. The line of apses advances, making one revolution in about 8.85 years. The node of the Moon's orbital plane (its intersection with the ecliptic) regresses in the ecliptic plane with a sidereal period of 6798.3 days (about 18.61 years); the node moving westward on the ecliptic at a rate of roughly 1° in 18.9 days. The regression of the lunar nodes is intrinsically related with the Saros cycle. This complexity of lunar motion must be taken into account for long-term studies of HAMR object dynamics.

To describe the motion of the Earth about the Sun, we define a heliocentric orbit frame, $(\hat{\mathbf{E}}_e, \hat{\mathbf{E}}_{e_\perp}, \hat{\mathbf{H}}_e)$, in which $\hat{\mathbf{E}}_e$ is the unit vector pointing to the orbit perihelion, $\hat{\mathbf{E}}_{e_\perp}$ is the unit vector in the heliocentric plane of motion and normal to $\hat{\mathbf{E}}_e$, and the cross product of these two vectors defines the orbit normal, specified as $\hat{\mathbf{H}}_e$, about which the Earth revolves.[1] With this formulation, the varying position vector between the Earth and the Sun is specified as $\mathbf{d}_e = d_e\hat{\mathbf{d}}_e$ and split into a magnitude d_e and a direction $\hat{\mathbf{d}}_e$, both of which are functions of the Earth true anomaly f_e

$$d_e = \frac{a_e(1-e_e^2)}{1+e_e\cos f_e}, \tag{1}$$

$$\hat{\mathbf{d}}_e = \cos f_e\hat{\mathbf{E}}_e + \sin f_e\hat{\mathbf{E}}_{e_\perp}, \tag{2}$$

where a_e and e_e are the semi-major axis and eccentricity of the Earth's heliocentric orbit, respectively.

The Moon's actual motion is very complex; high-precision lunar ephemerides are available through the Jet Propulsion Laboratory, which account for the relativistic n-body equations of motion for the point-mass Sun, Moon, planets, and major asteroids, perturbations on the orbit of the Earth–Moon barycenter from the interaction of the point-mass Sun with the figure, solid-body tides of both the Earth and Moon, and observations of lunar laser ranging (Folkner et al., 2009). Our purpose in this paper is to adopt the simplest possible expressions useful for studying the long-term evolution of HAMR debris orbits. These expressions must reveal the qualitative regularities of motion, and they must provide, with a certain degree of accuracy, a way of obtaining quantitative predictions of long-term changes. To that end, we assume that the Moon is on an osculating elliptical orbit in which the lunar node precesses clockwise in the ecliptic plane with a period of about 18.61 years. Note that we neglect the rotation of the lunar perigee as well as the periodic variations in the Moon's semi-major axis, eccentricity, and inclination. We define a geocentric orbit frame, $(\hat{\mathbf{E}}_m, \hat{\mathbf{E}}_{m_\perp}, \hat{\mathbf{H}}_m)$, where $\hat{\mathbf{E}}_m$ is the unit vector pointing to the orbit perigee, $\hat{\mathbf{E}}_{m_\perp} = \hat{\mathbf{H}}_m \times \hat{\mathbf{E}}_m$, and $\hat{\mathbf{H}}_m$ is the Moon's angular momentum unit vector, about which the Moon revolves. These vectors are resolved using the Moon's mean ecliptic orbital elements in which $\Omega_m(t) = \Omega_{m_0} + \dot{\Omega}_m(t-t_0)$, where $\dot{\Omega}_m = -2\pi/P_{\text{saros}}$ and P_{saros} is the sidereal period of nodal regression in seconds. The position vector from the Earth to the Moon is then be specified as $\mathbf{d}_m = d_m\hat{\mathbf{d}}_m$, where d_m and $\hat{\mathbf{d}}_m$ are given by Eqs. 1 and 2, respectively, using the Moon's orbit parameters.

[1] These are the orientation-defining integrals of the two-body problem, and can be specified using the classical orbital elements relative to an inertial frame (Scheeres, 2012a).

2.2. Solar radiation pressure

Solar radiation pressure is the largest non-gravitational perturbative force to affect the motion of HAMR objects in high-Earth orbits, causing extreme variations in their orbital parameters over short time periods. Typical analysis of long-term orbit dynamics models the SRP acceleration using the cannonball model, which treats the object as a sphere with constant optical properties (Valk et al., 2008; Anselmo and Pardini, 2010; Scheeres et al., 2011). The total momentum transfer from the incident solar photons is modeled as insolation plus reflection, and the force generated is independent of the body's attitude. Any force component normal to the object-Sun line that results from an aspherical shape or nonuniformly reflecting surface is thereby neglected. Then the net acceleration will act in the direction directly away from this line and have the general form (Scheeres, 2012a)

$$\mathbf{a}_{srp} = -(1+\rho)(A/m)P_\Phi\frac{(\mathbf{d}_s-\mathbf{r})}{|\,\mathbf{d}_s-\mathbf{r}\,|^3} \tag{3}$$

$$= -\beta\frac{(\mathbf{d}_s-\mathbf{r})}{|\,\mathbf{d}_s-\mathbf{r}\,|^3}, \tag{4}$$

where ρ is the reflectance, A/m is the appropriate cross-sectional area-to-mass ratio in m^2/kg, P_Φ is the solar radiation constant and is approximately equal to $1\times10^8\ \text{kg km}^3/\text{s}^2/\text{m}^2$, and $\beta = (1+\rho)(A/m)P_\Phi$. The vector from the Earth to the Sun is given by $\mathbf{d}_s = -\mathbf{d}_e$, and the position vector of the orbiter relative to the Earth is $\mathbf{r}$. This solar radiation pressure model can be rewritten as a disturbing function

$$\mathcal{R}_{srp} = -\beta\frac{1}{|\,\mathbf{d}_s-\mathbf{r}\,|}, \tag{5}$$

where $\mathbf{a}_{srp} = \partial\mathcal{R}_{srp}/\partial\mathbf{r}$. If the object is close to the Earth, or $r \ll d_s$, the disturbing function can be further simplified by expanding $1/|\,\mathbf{d}_s-\mathbf{r}\,|$ and keeping the first term that contains the position vector $\mathbf{r}$:

$$\mathcal{R}_{srp} = -\frac{\beta}{d_s^3}\mathbf{d}_s\cdot\mathbf{r}, \tag{6}$$

with the gradient giving a solar radiation pressure acceleration independent of the object's position relative to the Earth:

$$\mathbf{a}_{srp} = -\frac{\beta}{d_s^2}\hat{\mathbf{d}}_s. \tag{7}$$

The effects of the Earth's shadow are not taken into account; and as we are only considering distant Earth orbits, we also neglect Earth-albedo radiation pressure.

For a given semi-major axis, a, reflectivity, and A/m value, we define the SRP perturbation angle (first defined by Mignard and Hénon (1984)) as

$$\tan\Lambda = \frac{3\beta}{2}\sqrt{\frac{a}{\mu\mu_s a_e(1-e_e^2)}}, \tag{8}$$

where μ and μ_s are the gravitational parameters of the Earth and the Sun, respectively. We note that as the SRP perturbation becomes strong, $\Lambda \to \pi/2$; and as it becomes weak $\Lambda \to 0$. The angle Λ can be used to rigorously characterize the strength of the SRP perturbation acting on a body as a function of its orbit, its non-gravitational parameter, and the orbit of the Earth about the Sun. As it combines these quantities into a single parameter, which completely defines the long-term SRP-only solution (qq.v., Richter and Keller, 1995; Scheeres et al., 2011; Scheeres, 2012b), we find it efficacious to use as the fundamental defining characteristic of HAMR objects.

Although the cannonball model captures the general nature of SRP, it does not provide a precise prediction of how an individual object will evolve. However, this simple model is commonly used in the propagation of HAMR debris orbits since there is no method to incorporate a physically realistic SRP model with a lack of a priori information (i.e., object geometry, attitude behavior, surface properties, thermal characteristics, etc.). Even though the cannonball model may not realistically represent the SRP force acting on these objects, the fact that this model gives rise to many complex dynamical behaviors necessitates a deeper understanding of this basic model before exploring these more complex models. Thus, in the current paper, we will focus on the cannonball model as that will allow a direct comparison with earlier analyses of HAMR debris orbit dynamics (cf. Liou and Weaver, 2005; Chao, 2006; Valk et al., 2008; Anselmo and Pardini, 2010).

2.3. Earth mass distribution

We consider the effects of the C_{20} and C_{22} terms of the harmonic expansion of Earth's gravitational potential, which account for the polar and equatorial flattening of the Earth's figure. Inclusion of these predominant harmonics is sufficient to capture the main effects of nonsphericity in the Earth's mass distribution at high-altitude orbits. The standard way to represent the disturbing function of the second degree and order gravity field perturbation is using a body-fixed frame with latitude angle δ measured from the equatorial plane and longitude angle λ measured in the equator from the axis of minimum moment of inertia (Scheeres, 2012a)

$$\mathcal{R}_2 = -\frac{\mu C_{20}}{2r^3}\left(1-3\sin^2\delta\right) + \frac{3\mu C_{22}}{r^3}\cos^2\delta\cos 2\lambda, \tag{9}$$

where $C_{20} = -J_2 R_e^2$ is the dimensional oblateness gravity field coefficient, R_e is the mean equatorial radius of the Earth, and C_{22} is the dimensional ellipticity gravity field coefficient. We can state the disturbing function in a general vector expression

$$\mathcal{R}_2 = -\frac{\mu C_{20}}{2r^3}\left[1-3(\hat{\mathbf{r}}\cdot\hat{\mathbf{p}})^2\right] + \frac{3\mu C_{22}}{r^3}\left[(\hat{\mathbf{r}}\cdot\hat{\mathbf{s}})^2 - (\hat{\mathbf{r}}\cdot\hat{\mathbf{q}})^2\right], \tag{10}$$

where we assume that the unit vectors $\hat{\mathbf{p}}, \hat{\mathbf{q}}$, and $\hat{\mathbf{s}}$ are aligned with the Earth's maximum, intermediate, and minimum axes of inertia. The perturbing acceleration is then

$$\begin{aligned}\mathbf{a}_2 = {} & \frac{3\mu C_{20}}{2r^4}\left\{\left[1-5(\hat{\mathbf{r}}\cdot\hat{\mathbf{p}})^2\right]\hat{\mathbf{r}} + 2(\hat{\mathbf{r}}\cdot\hat{\mathbf{p}})\hat{\mathbf{p}}\right\} \\ & - \frac{3\mu C_{22}}{r^4}\left\{5\left[(\hat{\mathbf{r}}\cdot\hat{\mathbf{s}})^2 - (\hat{\mathbf{r}}\cdot\hat{\mathbf{q}})^2\right]\hat{\mathbf{r}} - 2[(\hat{\mathbf{r}}\cdot\hat{\mathbf{s}})\hat{\mathbf{s}} - (\hat{\mathbf{r}}\cdot\hat{\mathbf{q}})\hat{\mathbf{q}}]\right\}.\end{aligned} \tag{11}$$

2.4. Lunisolar gravitational attraction

Also necessary to incorporate in this analysis is the perturbation of the Sun and Moon's gravity on the motion of the HAMR object. These can be modeled as third-body perturbations, and their functional form can be simplified by performing an appropriate expansion. Taking Earth as the center of our dynamical system, the perturbation acceleration from a body with gravitational parameter μ_p is (Scheeres, 2012a)

$$\mathbf{a}_p = -\mu_p\left[\frac{\mathbf{r}-\mathbf{d}_p}{|\mathbf{r}-\mathbf{d}_p|^3} + \frac{\mathbf{d}_p}{|\mathbf{d}_p|^3}\right], \tag{12}$$

where $\mathbf{d}_p$ is the position vector of the perturbing body relative to Earth. For use in perturbation analysis it is convenient to recast this as a disturbing function

$$\mathcal{R}_p = \mu_p\left[\frac{1}{|\mathbf{r}-\mathbf{d}_p|} - \frac{\mathbf{d}_p\cdot\mathbf{r}}{|\mathbf{d}_p|^3}\right], \tag{13}$$

where $\mathbf{a}_p = \partial\mathcal{R}_p/\partial\mathbf{r}$. As the orbiter's distance from the Earth is small compared to the distance between the Earth and the third body, or $r/d_p \ll 1$, the disturbing function can be represented as an infinite series using the Legendre expansion, resulting in Scheeres (2012a)

$$\mathcal{R}_p = \frac{\mu_p}{d_p}\left[\sum_{i=0}^{\infty}\left(\frac{r}{d_p}\right)^i P_{i,0}\left(\frac{\mathbf{r}\cdot\mathbf{d}_p}{r d_p}\right) - \frac{\mathbf{d}_p\cdot\mathbf{r}}{d_p^2}\right]. \tag{14}$$

Keeping only the first non-constant term, with the Legendre polynomial $P_{2,0}(x) = 1/2(3x^2-1)$, yields

$$\mathcal{R}_p = \frac{\mu_p}{2d_p^3}\left[3(\mathbf{r}\cdot\hat{\mathbf{d}}_p)^2 - r^2\right]. \tag{15}$$

Thus, to lowest order, the gravitational attraction of the Sun and the Moon can be represented as a quadratic form, which is the fundamental approximation made in the Hill problem. Under this approximation, the perturbing acceleration simplifies to

$$\mathbf{a}_p = \frac{\mu_p}{d_p^3}\left[3(\mathbf{r}\cdot\hat{\mathbf{d}}_p)\hat{\mathbf{d}}_p - \mathbf{r}\right]. \tag{16}$$

2.5. Non-averaged Equations of Motion

Combining the above force models, we can define the equations of motion for a HAMR object in orbit about the oblate Earth disturbed by solar radiation pressure and lunisolar gravity. In an inertially fixed frame centered at the Earth, they can be stated in relative form

$$\ddot{\mathbf{r}} = \frac{\partial U}{\partial \mathbf{r}}, \tag{17}$$

$$U(\mathbf{r}) = \frac{\mu}{r} + \mathcal{R}_{srp}(\mathbf{r}) + \mathcal{R}_2(\mathbf{r}) + \mathcal{R}_s(\mathbf{r}) + \mathcal{R}_m(\mathbf{r}), \tag{18}$$

where $\mathcal{R}_s$ and $\mathcal{R}_m$ are third-body disturbing functions for the Sun and the Moon, respectively. Performing the partial derivatives, we can state the problem in terms of the perturbation accelerations as

$$\ddot{\mathbf{r}} = -\frac{\mu}{r^3}\mathbf{r} + \mathbf{a}_{srp} + \mathbf{a}_2 + \mathbf{a}_s + \mathbf{a}_m. \tag{19}$$

3. Averaged dynamics

We now introduce the concept of averaging as this allows us to evaluate the secular effects of the perturbations on our system. For averaging to be valid, we assume that the perturbing forces are sufficiently small so that, over one orbital period, the deviations of the true trajectory from the Keplerian trajectory are relatively small. In this case, oscillations in the orbital elements will average out over reasonably small periods. We refer the reader to Bogoliubov and Mitropolski (1961) for a theoretical discussion on the mathematical bases of averaging.

3.1. Milankovitch orbital elements

In his monumental work on the astronomical theory of paleoclimates, Milutin Milankovitch (1879–1958) reformulated the classical method of perturbation of elements using the two vectorial integrals of the unperturbed two-body problem–the angular momentum (areal) vector and the Laplace vector (Milankovitch, 1941). The vectorial integrals describe the spatial orientation, geometrical shape, and size of the osculating Keplerian orbit, and, together with the sixth scalar integral that represents the motion in time, constitutes a complete set of orbital elements. Geometrically, the angular momentum vector, $\mathbf{H}$, points perpendicular to the instantaneous orbit plane and the Laplace vector, $\mathbf{b} = \mu\mathbf{e}$, where $\mathbf{e}$ is the eccentricity vector, points towards the instantaneous periapsis of the orbit. At a more fundamental level, the vector $\mathbf{H}$ represents twice the areal velocity of the planet, and hence expresses Kepler's Second Law in vectorial form; the vector $\mathbf{b}$ can be interpreted as the equation for the hodograph of Keplerian motion (i.e., the shape of Keplerian trajectories in velocity or momentum space) (q.v., Battin, 1999). These elements have not been widely used in celestial mechanics in the past thirty years, and have recently been reformulated and expounded on in Rosengren and Scheeres (submited for publication).

The Milankovitch elements are particularly useful in finding the first-order long-period and secular variations by means of the Krylov–Bogoliubov–Mitropolski method of averaging (qq.v., Musen, 1960; Musen, 1961; Allan, 1962). When the disturbing function is limited to its secular part, in accordance with the method of averaging, the semi-major axis does not undergo any secular changes. Since the semi-major axis is secularly invariable, the angular momentum vector can be scaled by $\sqrt{\mu a}$. For this vector, denoted here as $\mathbf{h}$, together with the eccentricity vector, $\mathbf{e}$, the secular Milankovitch equations take a compact and symmetrical form. We can write these vectors in terms of the position, $\mathbf{r}$, and velocity, $\mathbf{v}$, in dyadic notation[2] as

$$\mathbf{h} = \frac{1}{\sqrt{\mu a}}\tilde{\mathbf{r}}\cdot\mathbf{v}, \tag{20}$$

$$\mathbf{e} = \frac{1}{\mu}\tilde{\mathbf{v}}\cdot\tilde{\mathbf{r}}\cdot\mathbf{v} - \frac{\mathbf{r}}{|\mathbf{r}|}. \tag{21}$$

The first-order averaged equations in Lagrangian form can be stated as (Allan and Cook, 1964; Tremaine et al., 2009; Rosengren and Scheeres, submited for publication)

$$\dot{\bar{\mathbf{h}}} = \tilde{\bar{\mathbf{h}}}\cdot\frac{\partial\bar{\mathcal{R}}^*}{\partial\bar{\mathbf{h}}} + \tilde{\bar{\mathbf{e}}}\cdot\frac{\partial\bar{\mathcal{R}}^*}{\partial\bar{\mathbf{e}}}, \tag{22}$$

$$\dot{\bar{\mathbf{e}}} = \tilde{\bar{\mathbf{e}}}\cdot\frac{\partial\bar{\mathcal{R}}^*}{\partial\bar{\mathbf{h}}} + \tilde{\bar{\mathbf{h}}}\cdot\frac{\partial\bar{\mathcal{R}}^*}{\partial\bar{\mathbf{e}}}, \tag{23}$$

where the over bar indicates the averaged value and $\bar{\mathcal{R}}^* = \bar{\mathcal{R}}(\bar{\mathbf{h}},\bar{\mathbf{e}})/\sqrt{\mu a}$. We note that the partials of $\bar{\mathcal{R}}^*$ are taken independently. The averaged disturbing function is defined as

$$\bar{\mathcal{R}}(\bar{\mathbf{h}},\bar{\mathbf{e}}) = \frac{1}{2\pi}\int_0^{2\pi}\mathcal{R}(\boldsymbol{\alpha}, M)\,\mathrm{d}M, \tag{24}$$

where $\boldsymbol{\alpha}$ is an arbitrary set of orbital elements excluding the mean anomaly, and $\bar{\mathcal{R}}(\bar{\mathbf{h}},\bar{\mathbf{e}})$ is independent of the fast variable M. Eqs. 22 and 23 admit two integrals $\bar{\mathbf{h}}\cdot\bar{\mathbf{e}}$ and $\bar{\mathbf{h}}\cdot\bar{\mathbf{h}} + \bar{\mathbf{e}}\cdot\bar{\mathbf{e}}$; physically meaningful solutions are restricted to the four-dimensional manifold on which $\bar{\mathbf{h}}\cdot\bar{\mathbf{e}} = 0$ and $\bar{\mathbf{h}}\cdot\bar{\mathbf{h}} + \bar{\mathbf{e}}\cdot\bar{\mathbf{e}} = 1$ (Tremaine et al., 2009).

Perturbation equations in terms of the Milankovitch elements in Gaussian form, that is, with the disturbing acceleration given explicitly, were used after their inception, most notably by Musen and Allan. Musen (1960) used these elements to study the effects of solar radiation pressure on the long-term orbit evolution of the Vanguard I satellite. Musen (1961) also developed secular equations for third-body perturbations, which are valid for all eccen-

[2] The notation $\tilde{\mathbf{a}}$ denotes the cross-product dyadic, defined such that $\tilde{\mathbf{a}}\cdot\mathbf{b} = \mathbf{a}\cdot\tilde{\mathbf{b}} = \mathbf{a}\times\mathbf{b}$. See Rosengren and Scheeres, submited for publication for a synopsis of the basic notation and properties of dyadics.

tricity and all inclination. The third-body disturbing function was truncated to the lowest-order term in the Legendre expansion (i.e., Hill's approximation), and averaged over the periods of both the orbiter and the disturbing body. Allan (1962) extended Musen's work by incorporating the parallactic term (third harmonic) into the disturbing function expansion. Because these equations are not widely known, and in order to draw attention to their applicability and elegance, we give here an outline of their derivations using the Lagrangian form of the secular Milankovitch equations. We also derive the secular equations resulting from Earth's oblateness (J_2), and combine them with the other perturbations to give a complete first-order averaged model for the evolution of HAMR debris in GEO.

3.2. Averaged SRP dynamics

Using the Lagrange planetary equations, the disturbing function can be averaged prior to application in this system. Substituting Eq. 6 into Eq. 24, we find

$$\bar{\mathcal{R}}_{srp} = \frac{1}{2\pi}\int_0^{2\pi} \mathcal{R}_{srp}\,\mathrm{d}M \tag{25}$$

$$= -\frac{\beta}{d_s^2}\hat{\mathbf{d}}_s \cdot \bar{\mathbf{r}}. \tag{26}$$

Thus, we only need to compute the average of the position vector, a classically known result[3]

$$\bar{\mathbf{r}} = -\frac{3}{2}a\mathbf{e}. \tag{27}$$

This leads to

$$\bar{\mathcal{R}}^*_{srp} = \frac{3}{2}\sqrt{\frac{a}{\mu}}\frac{\beta}{d_s^2}\hat{\mathbf{d}}_s \cdot \mathbf{e}. \tag{28}$$

Stated in this form, the scaled averaged disturbing function can be substituted into the secular Milankovitch equations, Eqs. 22 and 23, giving (cf. Richter and Keller, 1995)

$$\dot{\mathbf{h}}_{srp} = -\frac{3}{2}\sqrt{\frac{a}{\mu}}\frac{\beta}{d_s^2}\tilde{\hat{\mathbf{d}}}_s \cdot \mathbf{e}, \tag{29}$$

$$\dot{\mathbf{e}}_{srp} = -\frac{3}{2}\sqrt{\frac{a}{\mu}}\frac{\beta}{d_s^2}\tilde{\hat{\mathbf{d}}}_s \cdot \mathbf{h}. \tag{30}$$

Richter and Keller (1995) and Scheeres (2012b) showed that the averaged SRP equations, Eqs. 29 and 30, can be solved in closed form, yielding an analytical solution for the secular variation in the scaled angular momentum and eccentricity vectors. The analytical solution is expressed in a frame that rotates with the planet-Sun line, and solutions are periodic in $f_e/\cos\Lambda$, repeating every Earth true anomaly $2\pi\cos\Lambda$. Thus, over one heliocentric orbit the solution will advance $1/\cos\Lambda$ times. As the perturbation grows large, and Λ approaches $\pi/2$, the solution will repeat many times over one year. Conversely, as the perturbation grows small the solution will repeat only once every year.

In a previous study (q.v., Scheeres et al., 2011), we applied the SRP-only averaged solution to the dynamics of HAMR objects in GEO and GPS orbit regimes having a variety of Λ values. One of the surprising aspects of the theory is that the extremely simple, periodic behavior that occurs relative to the Earth-Sun rotating frame becomes quite complex and aperiodic in the Earth equatorial frame. The presence of the complex oscillations in the inclination and eccentricity vector, with short-period and long-period terms, is just an artifact of transforming into the inertial frame.

3.3. Averaged J_2 dynamics

Tesseral harmonics in the Earth's gravitational potential can also introduce long-term effects, especially if the mean motion of the object is commensurable with the angular velocity of Earth's rotation. The most interesting case is the influence of the ellipticity of Earth's equator on the motion of a geostationary object. This effect was studied by Lemaître et al. (2009) for HAMR objects in GEO space who found that a resonance occurs from the C_{22} dynamics, giving rise to chaotic behavior localized to a narrow range of semi-major axis. The averaged effect of this perturbation must be treated using a resonance theory. With mean motion averaging, our formulation will be unable to account for this subtle, and potentially important, aspect of motion. Therefore, we only consider the averaged C_{20} dynamics in our system. The averaged C_{22} dynamics will be studied in future work.

Performing the average over the second zonal harmonic disturbing function gives

$$\bar{\mathcal{R}}_{20} = -\frac{\mu C_{20}}{2}\left[\overline{\frac{1}{r^3}} - 3\hat{\mathbf{p}}\cdot\overline{\left(\frac{\hat{\mathbf{r}}\hat{\mathbf{r}}}{r^3}\right)}\cdot\hat{\mathbf{p}}\right], \tag{31}$$

where the product of two unit vectors, **ab**, is called a dyad and, in column and row vector notation is equivalent to the outer product (i.e., $[\mathbf{a}][\mathbf{b}]^T$). From Musen (1961), we have

$$\overline{\frac{1}{r^3}} = \frac{1}{a^3h^3}, \tag{32}$$

$$\overline{\left(\frac{\hat{\mathbf{r}}\hat{\mathbf{r}}}{r^3}\right)} = \frac{1}{2a^3h^3}\left[\mathbf{U} - \hat{\mathbf{h}}\hat{\mathbf{h}}\right], \tag{33}$$

where **U** is the identity dyadic and has the general property $\mathbf{U}\cdot\mathbf{a} = \mathbf{a}\cdot\mathbf{U} = \mathbf{a}$. Consequently,

$$\bar{\mathcal{R}}^*_{20} = \frac{nC_{20}}{4a^2h^3}\left[1 - 3(\hat{\mathbf{p}}\cdot\hat{\mathbf{h}})^2\right], \tag{34}$$

in which $n = \sqrt{\mu/a^3}$ is the orbiter's mean motion. Substituting $\bar{\mathcal{R}}^*_{20}$ into Eqs. 22 and 23, the secular equations for the oblateness gravity field perturbation can be written as

[3] The bar ($\bar{}$) operator is omitted from the Milankovitch elements in what follows because there is no ambiguity; i.e., all variables are averaged variables.

$$\dot{\mathbf{h}}_{20} = \frac{3nC_{20}}{2a^2h^5}(\hat{\mathbf{p}}\cdot\mathbf{h})\tilde{\hat{\mathbf{p}}}\cdot\mathbf{h}, \tag{35}$$

$$\dot{\mathbf{e}}_{20} = \frac{3nC_{20}}{4a^2h^5}\left\{\left[1-\frac{5}{h^2}(\hat{\mathbf{p}}\cdot\mathbf{h})^2\right]\tilde{\mathbf{h}} + 2(\hat{\mathbf{p}}\cdot\mathbf{h})\tilde{\hat{\mathbf{p}}}\right\}\cdot\mathbf{e}. \tag{36}$$

3.4. Averaged third-body dynamics

For the third-body perturbations, there are two timescales or frequencies over which the dynamical motion occurs. These timescales are defined by the orbital rate, n, and the motion of the perturbing body with its angular rate, N_p. If $N_p/n \ll 1$, it is acceptable to hold N_p constant while averaging over n; in which case, the remaining system has a time-varying term associated with N_p.

3.4.1. Singly-averaged equations

The Hill-approximated third-body disturbing function, Eq. 15, can be averaged over the orbiter's unperturbed two-body motion about the Earth as

$$\bar{\mathcal{R}}_p = \frac{\mu_p}{2d_p^3}\left[3\hat{\mathbf{d}}_p\cdot\overline{\mathbf{rr}}\cdot\hat{\mathbf{d}}_p - \overline{r^2}\right], \tag{37}$$

in which we note (Scheeres, 2012a)

$$\overline{r^2} = a^2\left(1+\frac{3}{2}e^2\right), \tag{38}$$

$$\overline{\mathbf{rr}} = \frac{1}{2}a^2\left[5\mathbf{ee} - \mathbf{hh} + (1-e^2)\mathbf{U}\right]. \tag{39}$$

Substituting Eqs. 38 and 39 into Eq. 37, and disregarding the irrelevant constant term, we have

$$\bar{\mathcal{R}}_p^* = \frac{3\mu_p}{4nd_p^3}\left[5(\hat{\mathbf{d}}_p\cdot\mathbf{e})^2 - (\hat{\mathbf{d}}_p\cdot\mathbf{h})^2 - 2e^2\right]. \tag{40}$$

From the secular Milankovitch equations, Eqs. 22 and 23, the singly-averaged third-body equations can be written in the form (cf. Allan, 1962)

$$\dot{\bar{\mathbf{h}}}_p = \frac{3\mu_p}{2nd_p^3}\hat{\mathbf{d}}_p\cdot(5\mathbf{ee}-\mathbf{hh})\cdot\tilde{\hat{\mathbf{d}}}_p, \tag{41}$$

$$\dot{\bar{\mathbf{e}}}_p = \frac{3\mu_p}{2nd_p^3}\left[\hat{\mathbf{d}}_p\cdot(5\mathbf{eh}-\mathbf{he})\cdot\tilde{\hat{\mathbf{d}}}_p - 2\tilde{\mathbf{h}}\cdot\mathbf{e}\right]. \tag{42}$$

3.4.2. Doubly-averaged equations

If the perturbing body is assumed to be in an elliptic orbit, and sufficient distance between the two timescales exists, then another averaging may be performed. Since averaging is a linear process, it can be performed over the secular Milankovitch equations directly to yield

$$\dot{\bar{\bar{\mathbf{h}}}}_p = \frac{1}{2\pi}\int_0^{2\pi}\dot{\bar{\mathbf{h}}}_p\,\mathrm{d}M_p \tag{43}$$

$$= -\frac{3\mu_p}{2n}\left[5\mathbf{e}\cdot\overline{\left(\frac{\hat{\mathbf{d}}_p\hat{\mathbf{d}}_p}{d_p^3}\right)}\cdot\tilde{\mathbf{e}} - \mathbf{h}\cdot\overline{\left(\frac{\hat{\mathbf{d}}_p\hat{\mathbf{d}}_p}{d_p^3}\right)}\cdot\tilde{\mathbf{h}}\right], \tag{44}$$

$$\dot{\bar{\bar{\mathbf{e}}}}_p = \frac{1}{2\pi}\int_0^{2\pi}\dot{\bar{\mathbf{e}}}_p\,\mathrm{d}M_p \tag{45}$$

$$= -\frac{3\mu_p}{2n}\left[5\mathbf{e}\cdot\overline{\left(\frac{\hat{\mathbf{d}}_p\hat{\mathbf{d}}_p}{d_p^3}\right)}\cdot\tilde{\mathbf{h}} - \mathbf{h}\cdot\overline{\left(\frac{\hat{\mathbf{d}}_p\hat{\mathbf{d}}_p}{d_p^3}\right)}\cdot\tilde{\mathbf{e}} + \overline{\left(\frac{1}{d_p^3}\right)}2\tilde{\mathbf{h}}\cdot\mathbf{e}\right], \tag{46}$$

where $(=)$ denotes the double averaged value. The average of these quantities are given by Eqs. 32 and 33. Consequently, the doubly-averaged third-body dynamics for an elliptically orbiting disturbing body become (cf. Musen, 1961)

$$\dot{\bar{\bar{\mathbf{h}}}}_p = -\frac{3\mu_p}{4na_p^3h_p^3}\hat{\mathbf{H}}_p\cdot(5\mathbf{ee}-\mathbf{hh})\cdot\tilde{\hat{\mathbf{H}}}_p, \tag{47}$$

$$\dot{\bar{\bar{\mathbf{e}}}}_p = -\frac{3\mu_p}{4na_p^3h_p^3}\left[\hat{\mathbf{H}}_p\cdot(5\mathbf{eh}-\mathbf{he})\cdot\tilde{\hat{\mathbf{H}}}_p - 2\tilde{\mathbf{h}}\cdot\mathbf{e}\right]. \tag{48}$$

where $\hat{\mathbf{H}}_p$ is the angular momentum unit vector of the perturbing body.

3.5. Secular equations of motion

The secular evolution of the Milankovitch orbital elements in the presence of SRP, J_2 and lunisolar perturbations can be stated as

$$\dot{\mathbf{h}} = \dot{\mathbf{h}}_{srp} + \dot{\mathbf{h}}_{20} + \dot{\mathbf{h}}_s + \dot{\mathbf{h}}_m, \tag{49}$$

$$\dot{\mathbf{e}} = \dot{\mathbf{e}}_{srp} + \dot{\mathbf{e}}_{20} + \dot{\mathbf{e}}_s + \dot{\mathbf{e}}_m, \tag{50}$$

where the over bar has been dropped, the SRP dynamics are given by Eqs. 29 and 30, and the C_{20} dynamics are given by Eqs. 35 and 36. The lunisolar dynamics can either be represented by the singly-averaged equations, Eqs. 41 and 42, or the doubly-averaged equations, Eqs. 47 and 48. In this formulation, the motion of the disturbing bodies can either be supplied from theory, i.e., the two-body solution, or can be provided by an ephemeris.

Combining all of these perturbations leads to a highly-nonlinear system, which does not appear integrable, but such simplifications help to understand some qualitative features of the system. Although the exact averaged solution is presumably inaccessible, the expressions given in Eqs. 49 and 50 are several hundred times faster to numerically integrate than their non-averaged Newtonian counterparts. With these results it is possible to predict accurately the long term orbital behavior of HAMR objects, given the initial values of the orbital elements and the initial geometry of the Earth–Moon–Sun system; the latter being important for calculation of Moon-induced perturbations.

Table 1
Maximum long-term inclination and minimum periapsis radius reached over all 360 trajectories for each SRP perturbation angle. The corresponding effective area-to-mass ratios are also listed. Recall that the Saros resonance becomes important between $\Lambda = 10.5^\circ$ and $\Lambda = 15.5^\circ$.

Λ [°]	$(1+\rho)A/m$ [m^2/kg]	max i [°]	min r_p [R_e]
0.85	1.36	15.40	6.4
4.26	6.8	19.79	5.6
8.47	13.6	28.56	4.6
12.60	20.4	39.64	3.7
13.81	22.44	48.04	3.3
16.59	27.2	41.21	2.9
20.43	34.0	43.88	2.2
24.08	40.8	44.28	1.5
27.54	47.6	48.03	1.0

4. Long-term dynamics of HAMR objects

Numerical integration of the precise non-averaged equations of motion represents the most accurate means of calculating the exact trajectory of an orbiting body in a given time interval. Anselmo and Pardini have made several numerical investigations of the HAMR debris problem, mapping out the dynamics of these objects over long timespans with all relevant perturbations included. Their most recent work presents a detailed analysis concerning the long-term evolution of HAMR debris in high-Earth orbit subject to SRP with Earth's shadow effects, geopotential harmonics up to degree and order eight, and third-body gravitational interactions induced by the Sun and the Moon (Anselmo and Pardini, 2010). Comparison of these solutions with the results obtained from the averaged formulas is a significantly reliable estimate of the accuracy of the approximated equations. Such comparison permits us to conclude about the applicability of the averaged equations for considering the evolution of HAMR debris orbits.

We restrict our attention to objects released in geostationary orbit ($a \sim 42164.2$ km) on 1950 January 01 12:00:00 UTC; therefore, $\mathbf{e}_0 \equiv \mathbf{0}$ and $\mathbf{h}_0 \equiv \hat{\mathbf{p}}$ (Earth's rotation pole). To understand the main characteristics of motion and to determine the extent to which the qualitative properties of the orbit persist with increasing area-to-mass, the dynamics were simulated using a reflectance value of 0.36, and area-to-mass ratios between 0 and 40 m^2/kg. For a given semi-major axis, reflectivity, and A/m value, we compute the corresponding Λ angle (Eq. 8), which we use to characterize the evolutionary behavior of HAMR debris orbits. The SRP perturbation angles and corresponding effective area-to-mass ratios are shown in Table 1.

4.1. Newtonian non-averaged dynamics

For the non-averaged dynamics, we use the high-accuracy Solar System ephemeris (DE421), provided by JPL, to calculate the position vectors of the Sun and the Moon (Folkner et al., 2009). The long-term orbit evolution of several HAMR objects, obtained using numerical integrations of the Newtonian equations of motion (Eq. 19), are shown in Fig. 1. The eccentricity and inclination evolution, over 100 years, shown in Figs. 1(a) and 1(b), closely match the results obtained by Anselmo and Pardini (2010).[4] For the object with $\Lambda = 12.60^\circ$ (corresponding to $(1+\rho)A/m = 20.4$ m^2/kg), the eccentricity undergoes an approximately yearly oscillation with amplitude of about 0.4 and long-period modulations of ~ 0.05. The inclination undergoes approximately yearly oscillations that are superimposed on the long-term drift, which has a varying maximum amplitude between 25° and 35° and a long-term oscillation period of about 22 years. As shown in Fig. 1(c), the evolution of the two-dimensional eccentricity vector, $e[\cos\omega\cos\Omega - \cos i\sin\omega\sin\Omega; \cos\omega\sin\Omega + \cos i\sin\omega\cos\Omega]$, is characterized by both a yearly and long-term regression; the latter exhibiting complex evolutionary behavior. The orbit pole, $\hat{\mathbf{h}}$, precesses clockwise, having the same characteristics as the inclination oscillation (see Fig. 1(d)).

4.2. Averaged dynamics

Since our Newtonian non-averaged results compare well, both quantitatively and qualitatively, with those of Anselmo and Pardini (2010),[5] they can be used as a logical basis for assessing the validity of our averaged model. We are particularly interested in distinguishing between cause and effect and in identifying the precise origin of any perturbation experienced by the HAMR object. To that end, we avoid using the precise JPL ephemeris, and instead assume two-body dynamics for the Sun and the Moon, for which the lunar node regresses in the ecliptic plane with a sidereal period of ~ 18.61 years (see Section 2.1).

The evolution of several HAMR objects, obtained using numerical integrations of the singly-averaged equations of motion, are shown in Fig. 2. The eccentricity evolution in Fig. 2(a) is shown over a shorter timescale to emphasize the respective amplitudes of the yearly oscillations for each object. The approximated averaged equations, using two-body dynamics and accounting for the regression of the Moon's node, gives us nearly identical plots at this level of resolution as the full Newtonian non-averaged simulations. We do not use any special formalism in our integrations to preserve the constraints on $\mathbf{h}$ and $\mathbf{e}$,[6] yet after 100 years, they are satisfied to over one part per billion.

With the Newtonian non-averaged formulation, the various perturbations are all lumped together and we obtain no indication as to the form and nature of any of them.

[4] Note that we used slightly different initial conditions and a different release epoch for our simulations; the latter will change the initial dynamical configuration of the Earth–Moon–Sun system.

[5] In addition to our force model, they account for higher-order gravity field perturbations and Earth shadow effects in their numerical integrations.

[6] Recall that $\mathbf{e}\cdot\mathbf{h} = 0$ and $\mathbf{e}\cdot\mathbf{e} + \mathbf{h}\cdot\mathbf{h} = 1$.

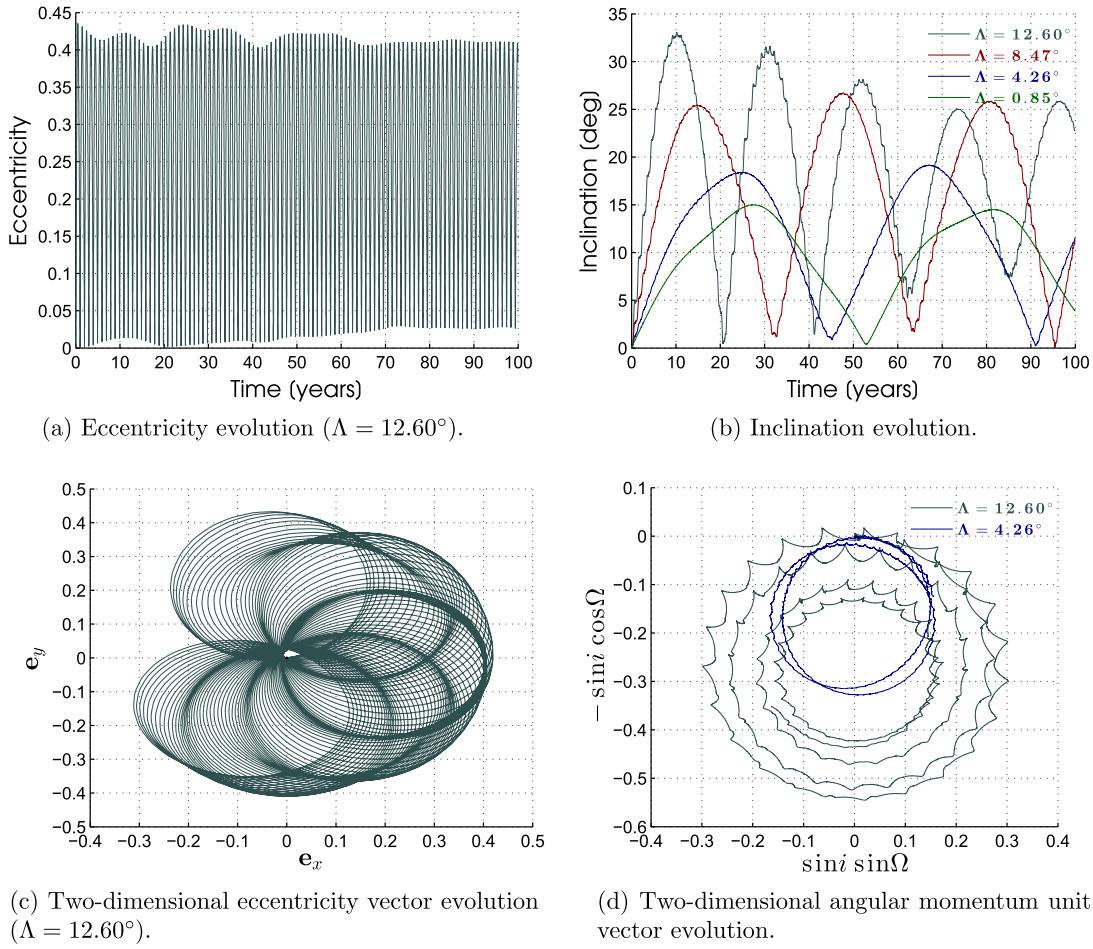

(a) Eccentricity evolution ($\Lambda = 12.60°$).

(b) Inclination evolution.

(c) Two-dimensional eccentricity vector evolution ($\Lambda = 12.60°$).

(d) Two-dimensional angular momentum unit vector evolution.

Fig. 1. Long-term orbit evolution (100 years) in the Earth-equatorial frame for different values of the SRP perturbation angle, as predicted by the full non-averaged equations of motion, Eq. 19, using Eq. 5 for SRP, Eq. 11 for C_{20} and C_{22}, and Eq. 12 for lunisolar perturbations. The position vectors of both the Sun and the Moon were computed using the JPL ephemeris (DE421).

However, our averaged formulation gives significant qualitative indications and allows us to understand many aspect of HAMR debris motion. Concerning the eccentricity evolution, solar radiation pressure acting alone induces sub-yearly oscillations with period $2\pi\cos\Lambda$; the amplitude increasing with increasing Λ. Inclusion of the C_{20} dynamics causes only slight changes in the short-term oscillations, but induces long-period small fluctuations in the maximum amplitudes. The dynamical coupling between SRP and oblateness becomes more pronounced with increasing Λ (q.v., Rosengren and Scheeres, 2011). The addition of third-body perturbations, primarily the attraction of the Moon, causes a slight increase in the short-term amplitudes, and gives rise to long-term aperiodic oscillations in the maximum amplitudes. Regarding the inclination evolution, solar radiation pressure accounts for the sub-yearly oscillations that ride on top of the longer-term secular drift, and the reduction in the long-term oscillation periods with increasing Λ (see Fig. 3). The addition of Earth oblateness brings about a reduction in both the amplitude and period of the long-term oscillations. Inclusion of lunisolar perturbations causes a slight increase in the long-term amplitudes and a decrease in the long-term oscillation periods, and for certain values of Λ—most notably $\Lambda = 12.60°$ (corresponding to $(1+\rho)A/m = 20.4\ \mathrm{m}^2/\mathrm{kg}$)—causes large fluctuations (peak-to-peak changes) in the maximum amplitudes. These fluctuations manifest themselves as a beating phenomenon in the evolution of the two-dimensional angular momentum unit vector, $[\sin i \sin\Omega, -\sin i \cos\Omega]$. Note that for lower values of Λ, this complex behavior is not observed, as shown in Fig. 2(b). The origin of this phenomenon, which also appears in the numerical results of Anselmo and Pardini (2010), will be discussed in Section 4.3.

The limitations and domain of validity of the doubly-averaged third-body equations (Eqs. 47 and 48), is discussed extensively in Rosengren and Scheeres (2012), and the relevant figures will be omitted here. Note that in all cases considered, the doubly-averaged equations predict the qualitative nature of the orbits; however, the angular momentum vector evolution becomes misaligned with the singly-averaged results after several decades. For larger SRP perturbation angles, corresponding to faster preces-

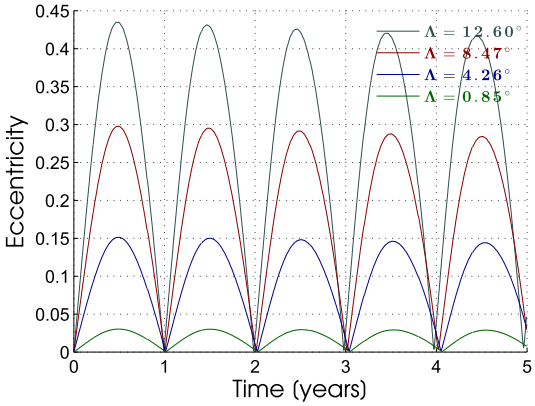

(a) Eccentricity evolution.

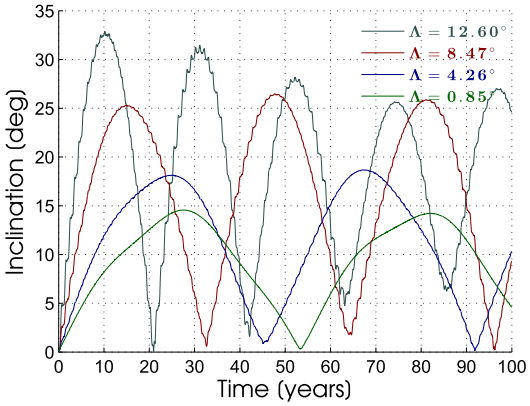

(b) Inclination evolution.

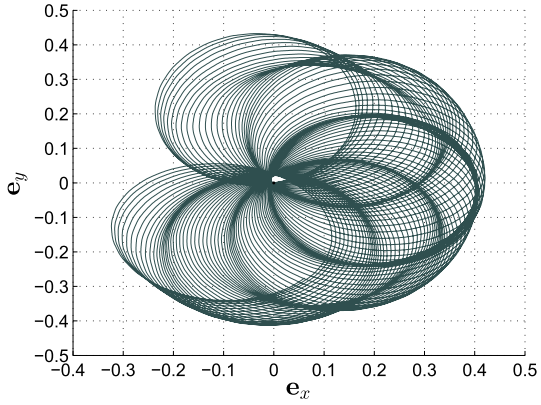

(c) Two-dimensional eccentricity vector evolution ($\Lambda = 12.60°$).

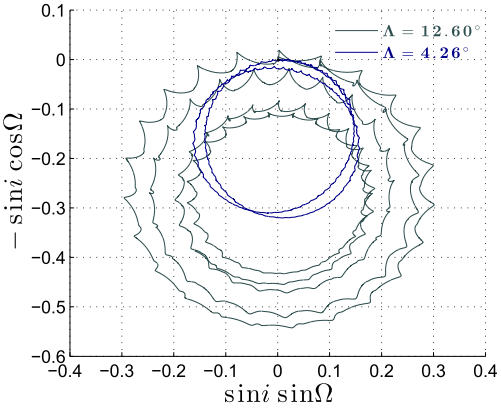

(d) Two-dimensional angular momentum unit vector evolution.

Fig. 2. Long-term orbit evolution in the Earth-equatorial frame for different values of the SRP perturbation angle, as predicted by the singly-averaged equations of motion, Eqs. 49 and 50, using Eqs. 29 and 30 for SRP, Eqs. 35 and 36 for C_{20}, and Eqs. 41 and 42 for lunisolar perturbations. The position vectors of both the Sun and Moon were computed using two-body dynamics, accounting for lunar nodal regression.

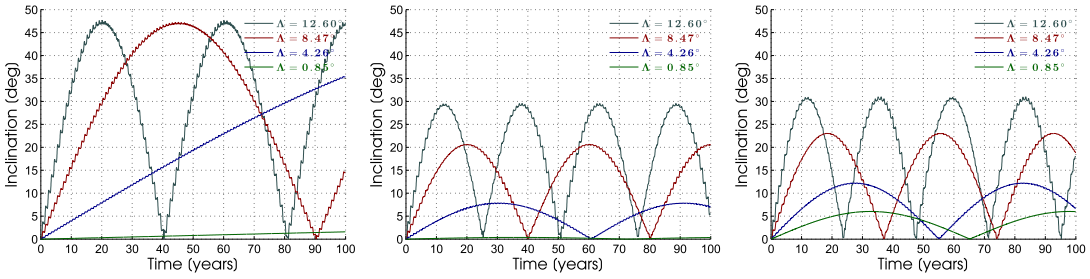

(a) SRP-only (b) SRP and oblateness (c) SRP, J_2, and solar gravity

Fig. 3. Accumulation of the effects on the long-term inclination evolution, as each perturbing force is added to the system.

sions of the angular momentum vector, this deviation becomes more pronounced. For $\Lambda = 12.60°$, the doubly-averaged equations are able to capture the complex beating phenomenon, but predict a faster precession causing a shift in the inclination evolution. In our derivation of the doubly-averaged equations, we assumed the Moon followed a Keplerian ellipse about the Earth; however, as the Moon's node regresses in the ecliptic plane, this assumption actually violates the averaging principle. As will become apparent in the following section, a resonance theory is needed in order to average out the Moon's motion for lunar third-body perturbations.

4.3. Saros secular resonance

The epoch date determines the initial geometry of the Earth–Moon–Sun system, and thus the initial location of the lunar ascending node. We found that when the nodal rate of the perturbed system is commensurate with the nodal rate of the Moon (i.e., the Saros), the perturbations build up more effectively over long periods to produce significant resonant effects on the orbit (Rosengren and Scheeres, 2012). Such resonances, which occur for a class of HAMR objects that are not cleared out of orbit through their eccentricity growth, gives rise to strongly changing dynamics over longer time periods. This resonant behavior explains the long-term beating phenomenon that occurs for $\Lambda = 12.60^\circ$ (see Fig. 2(b)). Its nodal period in the equatorial frame is close enough to the Saros (sidereal period of lunar nodal regression) that there is a strong interaction between the lunar effects and the overall precession rate.

Figs. 4–6 show the inclination and two-dimensional angular momentum vector evolution in the Earth equatorial frame, for several HAMR objects propagated using the same initial conditions, but varying the initial lunar node. Varying the initial location of the Moon's ascending node over 2π is, in a sense, equivalent to varying the release epoch within a Saros cycle. For $\Lambda = 13.81^\circ$, the nodal period in the equatorial frame is approximately equal to 18.61 years, thereby inducing a $1:1$ resonance with the Saros. The qualitative picture of the evolution changes drastically based on this angle, which is indicative of resonance. Figs. 5 and 6 show the evolution of objects with nodal rates either too slow or too fast to resonantly interact with the Saros. Note that for these objects, their orbits will change quantitatively based on the initial node angle, but the qualitative evolution remains the same. The approximate range of SRP perturbation angles for which resonance can be important at GEO is between $\Lambda = 10.5^\circ$ and $\Lambda = 15.5^\circ$ (corresponding to 16.93 $m^2/kg \leqslant (1+\rho)A/m \leqslant 25.33$ m^2/kg). We refer the reader to Rosengren and Scheeres (2012) for more details on the Saros resonance phenomenon.

4.4. Global behavior of HAMR debris

4.4.1. The classical Laplace plane

Almost fifty years have elapsed since satellites were first launched into geostationary orbit. The orbital dynamics of uncontrolled GEO satellites is governed by the oblateness of the Earth and third-body gravitational interactions

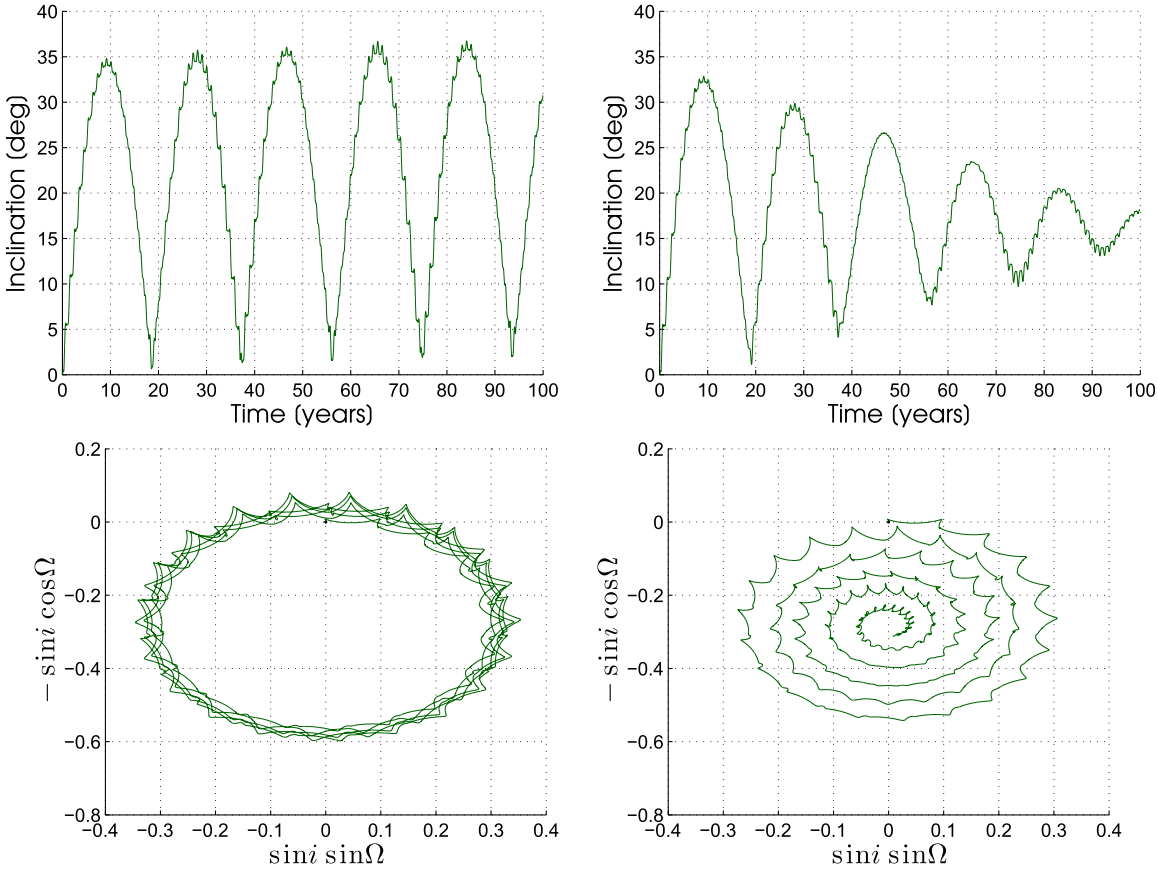

(a) $\Omega_m(0) = \Omega_{m_0}$. (b) $\Omega_m(0) = \Omega_{m_0} + 3\pi/2$.

Fig. 4. Long-term orbit evolution in the Earth-equatorial frame of an object with $\Lambda = 13.81^\circ$, as a function of the initial lunar node. Note the significant resonant effect caused by the Saros.

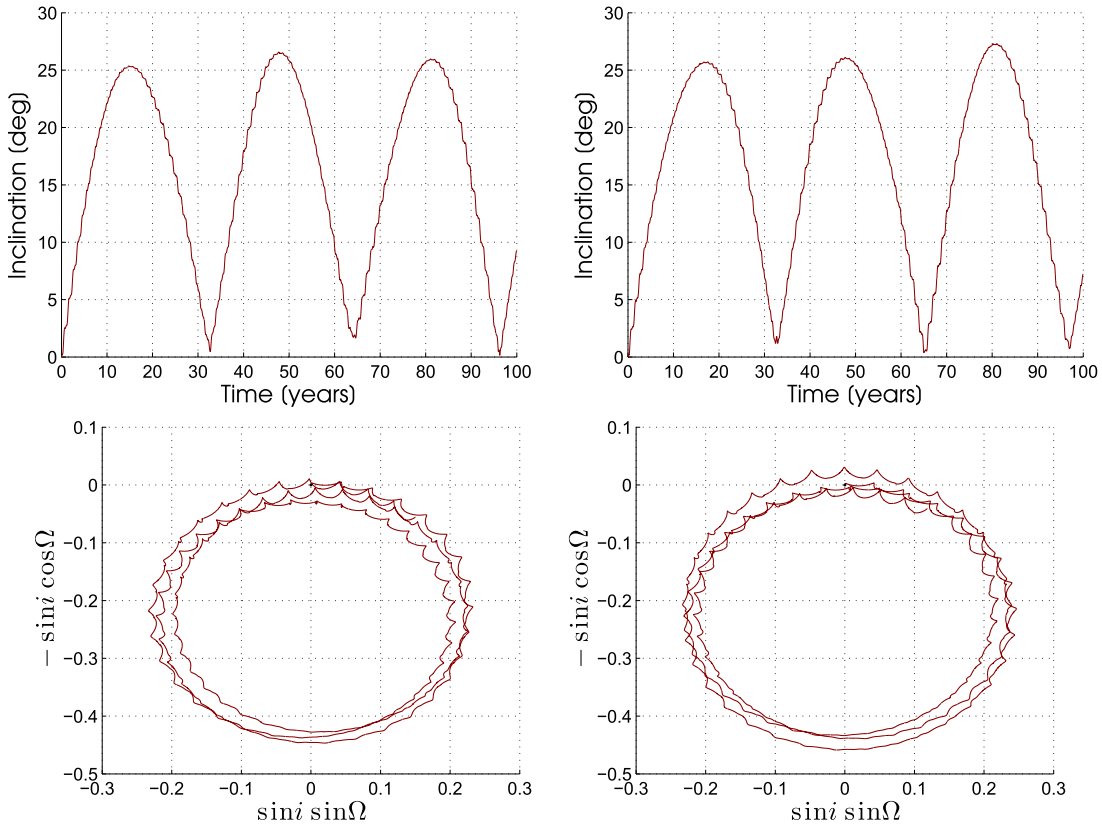

(a) $\Omega_m(0) = \Omega_{m_0}$. (b) $\Omega_m(0) = \Omega_{m_0} + 3\pi/2$.

Fig. 5. Long-term orbit evolution in the Earth-equatorial frame of an object with $\Lambda = 8.47°$, as a function of the initial lunar node. Note that the Saros resonance is not observable.

induced by the Sun and the Moon. By itself, Earth's oblateness causes the pole of the orbital plane to precess around the pole of Earth's equator, the rate of rotation being proportional to $J_2(R/a)^2 n$ (as can be seen from Eq. 35). Lunisolar perturbations will have a similar effect, but the precession will now take place about the poles of the orbital planes of the Moon and the Sun, respectively, at a rate proportional to n_p^2/n (see Eq. 47). The motion of the orbit pole of the satellite is a combination of simultaneous precession about these three different axes, one of which, the pole of the Moon's orbit, regresses around the pole of the ecliptic with a period of 18.61 years. The classical Laplace plane (or Laplacian plane) is the mean reference plane about whose axis the satellite's orbit precesses. On the Laplace place, the secular orbital evolution driven by the combined effects of these perturbations is zero, so that the orbits are "frozen." Under the approximation that the lunar orbit lies in the ecliptic, we can defined the Laplace plane at GEO, which lies between the plane of the Earth's equator and that of the ecliptic and passes through their intersection (i.e., the Vernal equinox), and which has an inclination of about 7.5° with respect to Earth's equator (Allan and Cook, 1964).

The significance of the classical Laplace plane is that the pole of an orbit inclined at a small angle to it will regress around the pole of this plane at nearly constant rate and inclination. This implies that the orbital planes of uncontrolled GEO satellites evolve in a systematic way; that is, their inclinations and ascending nodes are highly correlated. Shown in Fig. 7 is the long-term evolution of the inclination and ascending node, in the Earth equatorial frame, of initially geostationary satellites (note that SRP causes only negligible effects for a typical satellite). These inactive satellites precess at a nearly constant inclination about the pole of the Laplace plane with a period of about 54 years (q.v., Schildknecht, 2007). The maximum values of inclination occur at $\Omega = 0°$ (i.e., the ascending node of the Sun's orbit) and the minimum values occur at $\Omega = 180°$ (i.e., the descending node).

4.4.2. The modified Laplace plane

The natural question arises as to whether the inclination and ascending node for HAMR objects, which have area-to-mass ratios hundreds or thousands of times greater than that of a typical satellite and are thus strongly perturbed by solar radiation pressure, is also systematic (strongly correlated). It has been noted by Anselmo and Pardini (2010) that an increase in area-to-mass ratio leads to a faster and wider clockwise precession of the orbit pole. Tamayo et al. (2013) argues, in the context of circumplanetary dust

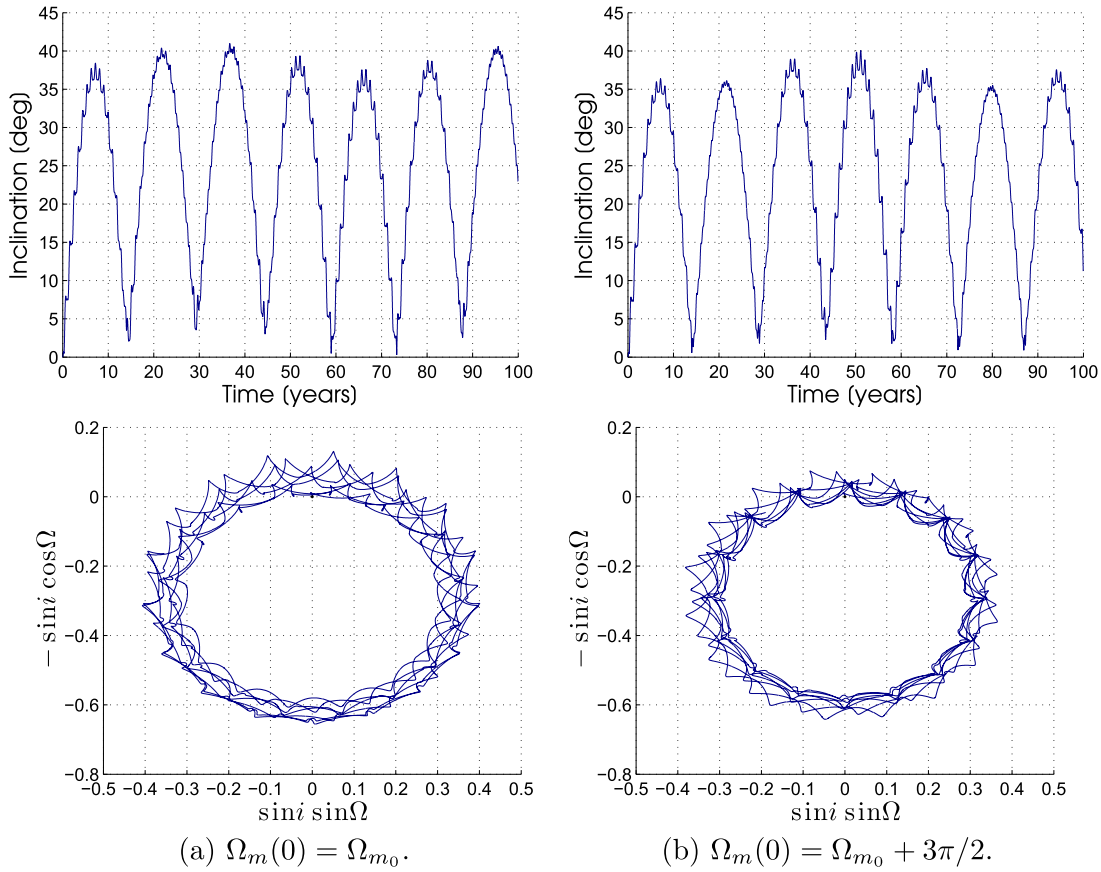

Fig. 6. Long-term orbit evolution in the Earth-equatorial frame of an object with $\Lambda = 16.59°$, as a function of the initial lunar node. Note that the Saros resonance is not observable.

particles, that solar radiation pressure modifies the classical Laplace plane equilibrium. In fact, Allan and Cook (1967), in considering the possibility of a geocentric contribution to the zodiacal light, show that solar radiation pressure acting alone causes a secular precession of the orbit around the pole of the ecliptic. They find an approximate solution

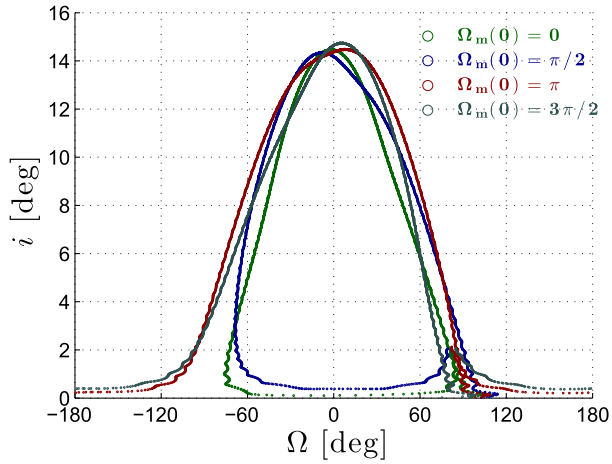

Fig. 7. Scatter plot of the time-series, over 54 years, of inclination and ascending node of initially geostationary objects subject to gravitational perturbations, as predicted by the averaged model. The long-term motion of the orbital plane is shown for four different initial positions of the lunar node, i.e., four different launch dates.

to the modified Laplace plane and note that the orbital plane of a given dust particle, for a given semi-major axis, will regress around this plane. However, the validity of their analysis is limited to dust particles that are only weakly perturbed by solar radiation pressure; that is, particles which have low values of effective area-to-mass ratio.

To understand the spatial distribution of the HAMR debris population, and to determine whether their (i, Ω) pattern is systematic, we investigated a range of HAMR objects, released in geostationary orbit with area-to-mass ratios from 0 up to 40 m^2/kg. We propagated over 80 different Λ values for 100 years, uniformly distributed in initial lunar node (360 different node values from 0 to 2π), giving nearly 30,000 simulations. As evident from Figs. 4–6, the initial location of the lunar node is an important parameter as different behavior occurs depending on where the object is relative to the Moon. Moreover, the initial lunar node can be correlated with any epoch within a Saros cycle, and thus may shed insight into the source of this debris.

Fig. 8 shows the time-series, over 100 years, of inclination and right ascension of the ascending node in the Earth-equatorial frame, for a range of SRP perturbation angles, for two trajectories selected out of the 360 different trajectories that are a function of the initial lunar node. That is, we track the statistics over all 360 initial lunar

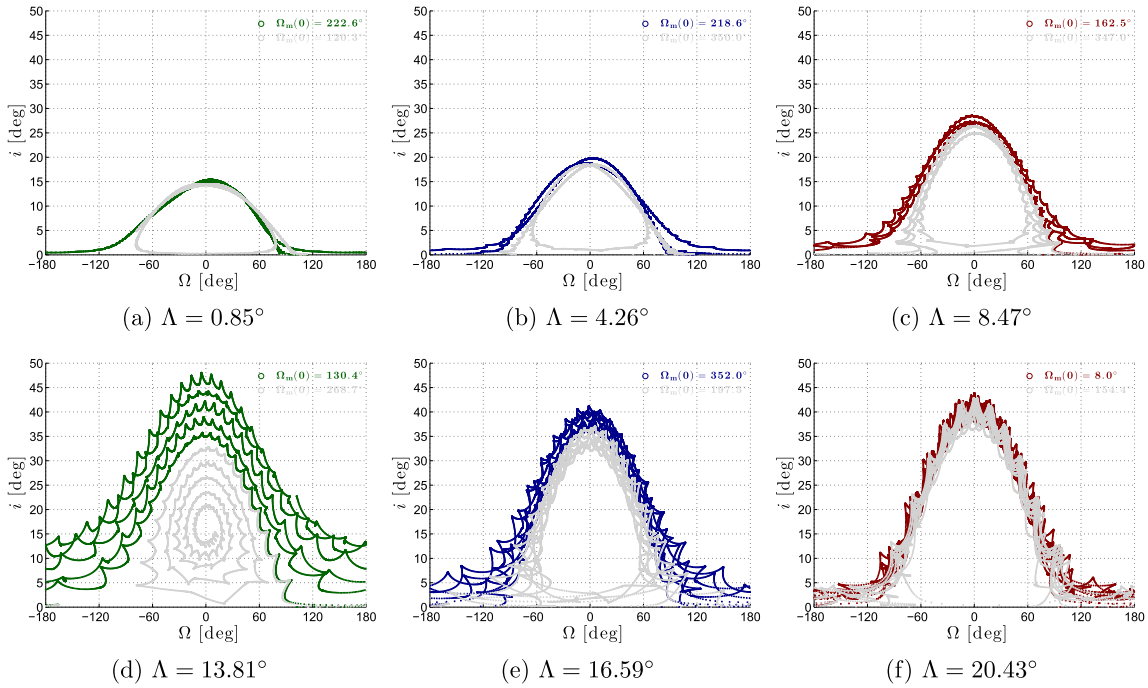

Fig. 8. Scatter plot of the time-series, over 100 years, of inclination and right ascension of the ascending node, for two selected trajectories for each value of Λ. The long-term motion of the orbital plane is shown for two different initial positions of the lunar node for each HAMR object, corresponding to the respective extreme cases.

nodes, and show the evolution which gives the largest value in maximum long-term inclination reached, and the evolution which gives the smallest value in maximum long-term inclination reached. Note that the initial node angles that produces these extreme cases will differ depending on the Λ angle. The maximum long-term inclination reached for each HAMR object is given in Table 1. For the non-Saros resonant objects, the qualitative behavior is the same with the maximum long-term inclination increasing with increasing Λ. The 1 : 1 Saros resonance for $\Lambda = 13.81^\circ$ can be observed in Fig. 8(d), and leads to this object having the largest maximum inclination across all Λ angles. In all cases, the pattern associated with their distribution in inclination and ascending node phase space is systematic (i.e., strongly correlated), which means that HAMR objects evolve in predictable ways. The systematic structure of the orbital planes for HAMR objects also implies that the classical Laplace plane can be generalized to accommodate solar radiation pressure (q.v., Allan and Cook, 1967). SRP will modify the classical Laplace plane, increasing its inclination relative to the equator with increasing Λ; each HAMR objects has its own modified Laplace plane for a given semi-major axis and effective area-to-mass ratio.

The orbital lifetime of HAMR objects is determined by their eccentricity growth and hence the decrease of their orbit perigee radius. An eccentricity above 0.849 for a semi-major axis corresponding to GEO would result in an impact with the Earth. Note that an object occupying this critical eccentricity orbit may not impact the Earth, if the eccentricity changes rapidly enough. Table 1 lists the lowest minimum periapsis reached across all 360 trajectories for each SRP perturbation angle. For a value of $\Lambda = 28.21^\circ$ ($(1+\rho)A/m = 49.0\ \mathrm{m}^2/\mathrm{kg}$), all 360 trajectories result in an eccentricity growth above 0.849 in less than a year, which should lead to shorter lifetimes for this debris. However, if the object does not go through perigee when the critical eccentricity is reached, it could persist in orbit for several decades. The results obtained are consistent with those of Anselmo and Pardini (2010). These limits may actually serve as a test for where such HAMR debris originated, but a more complete understanding of how the maximum eccentricity of a debris varies over time would need to be made.

5. Discussion

5.1. Accuracy of averaged equations

For our averaged model, the disturbing function was limited to the cannonball model of SRP without Earth shadow effects, the dominant zonal harmonic in the harmonic expansion of Earth's gravitational potential, and the lowest-order term in the Legendre expansion of the lunar and solar disturbing functions (i.e., Hill's approximation). Under these approximations, the semi-major axis does not undergo any secular changes and the problem reduces to understanding the remaining four orbital elements, e, i, Ω, and ω, at a given semi-major axis. For geosynchronous orbits, the tesseral harmonics in the geopotential coupled with solar radiation pressure can introduce long-term changes and even chaotic behavior in the semi-major axis (Lemaître et al., 2009). Hubaux et al. (2013) have demon-

strated that the Earth shadow effects, and even the precise model of shadow, can drastically modify the chaotic zone. However, these effects are localized to a narrow range of semi-major axis (hundreds of meters) and will not significantly affect the long-term orbit evolution. Indeed, even a 100 km change in semi-major axis will cause only a 0.1 percent change in the SRP perturbation angle.

The dynamical behavior underlined by our averaged model is in good agreement with earlier researchers (cf. Liou and Weaver, 2005; Chao, 2006; Valk et al., 2008; Anselmo and Pardini, 2010). We attribute any quantitative differences between the singly-averaged and non-averaged simulations to our use of the Hill approximation for the lunar perturbing potential; namely, in the assumption that $r/d_m \ll 1$. Since geosynchronous orbits are relatively small in comparison with that of the Earth and the Moon, only the first non-constant term needs to be retained in the Legendre expansion of the third-body disturbing function to obtain a good representation of the object's motion. However, since HAMR objects are in highly-eccentric GEO orbits, higher-order terms in the lunar disturbing function expansion may become important. Lidov (1962) showed that the parallactic term (third harmonic) can cause the eccentricity to build up more rapidly if the orbit is sufficiently large. In particular, the parallactic term becomes effective when the object is at a distance of about 10 Earth radii. Thus, we find that for an initial orbit at GEO semi-major axis, if the object has an eccentricity greater than 0.5, which occurs for $\Lambda > 15^\circ$, the parallactic term may need to be considered. A recursive formulation of the averaged third-body equations, such as that presented in Allan (1962), could be used to determine the effects of the parallactic term on the long-term orbital dynamics of HAMR objects; however, this will not be pursued here.

5.2. Saros resonance phenomenon

The recognition of the Saros resonance raises many questions of interest concerning the nature and evolution of the HAMR debris population. This phenomenon actually appears in the numerical results of Anselmo and Pardini (2010), and is relevant for many of the observed HAMR debris in near GEO orbits. Since the singly-averaged results capture this subtle behavior, our averaged model accounts for the full dynamics precisely, and can be used for accurate long-term predictions. Further analysis is needed to fully understand the resonance effect, and will be pursued in future research.

5.3. Systematic structure in (i, Ω) phase space

Observers are interested in knowing what the best search strategy is to maximize the detection efficiency of HAMR objects for future surveys. From this point of view, the distribution in (i, Ω) phase space indicates exactly where their surveys should concentrate. The systematic orientation of the orbital planes indicates that an anti-solar direction survey should concentrate near the equator during the spring and fall. During the summer and winter, the observers should look at high latitudes for highly inclined objects.

The distribution in inclination and ascending node phase space for HAMR objects subject to SRP, Earth oblateness, and lunisolar third-body gravitational interactions is the same systematic structure that the uncontrolled GEO satellite population exhibits. For inactive satellites, the oblateness of the Earth and the gravitational pull from the Moon and the Sun force their orbital planes to precess around the classical Laplace plane with a period of about 54 years (Allan and Cook, 1964; Schildknecht, 2007). Qualitatively, solar radiation pressure will have a precisely similar effect as solar gravitational perturbations, causing the orbit to precess around the pole of the ecliptic, the rate of rotation being proportional to $(1 - \cos\Lambda)/\cos\Lambda$. This can be inferred from the fact that the secular motion of an orbiter subject only to SRP is periodic in a frame rotating with the Earth's heliocentric true anomaly, and results from the forced precession of this periodic solution relative to an inertial frame (Scheeres, 2012b). Therefore, solar radiation pressure will modify the classical Laplace plane, increasing its equatorial inclination with increasing Λ (cf. Allan and Cook, 1967).

It is currently believed that HAMR objects are sheets of multilayer insulation detaching from payloads or buses of objects in the GEO disposal orbit due to material degradation in the space environment (Liou and Weaver, 2005). The modified Laplace plane will allow for the identification of robust, long-term GEO disposal orbits. It also has many implications for the planetary science community and may lead to a better understanding of the origin and evolution of natural satellites and binary asteroids, vide Tremaine et al. (2009).

6. Conclusions

We presented a complete non-singular formulation of first-order averaging explicitly given in terms of the Milankovitch elements–the scaled angular momentum vector and the eccentricity vector. This theory provides a unified approach to the analysis and simulation of HAMR debris over long timespans, and allows for the qualitative nature of their evolution to be understood. We exposed the Saros resonance as an important phenomena that has not been identified previously, and which leads to complex evolutionary behaviors when the perturbing forces act in concert. This resonance may play a role in generating orbital chaos, which is a topic of future research.

We have shown that we understand many aspect of HAMR debris motion, and that by knowing the complete qualitative picture of the evolution, we can use our model to predict the population. We applied the non-singular theory of first-order averaging toward an understanding of the general nature and spatial distribution of the HAMR debris population. We identified a systematic structure associ-

ated with their distribution in inclination and ascending node phase space, and discussed how it can be used to aid the space surveillance community in future search campaigns.

Acknowledgements

We would like to thank Alessandro Rossi and two anonymous referees for their lucid and thoughtful reports of our work. This material is based upon work supported by the National Science Foundation Graduate Research Fellowship under Grant No. DGE 1144083. Any opinions, findings, and conclusions or recommendations expressed in this material are those of the authors and do not necessarily reflect the views of the National Science Foundation. Daniel J. Scheeres acknowledges support from grant FA9550-11-1-0188, administered by the Air Force Office of Scientific Research.

References

Allan, R.R. Satellite orbit perturbations due to radiation pressure and Luni-solar forces. Q. J. Mech. Appl. Math. 15 (3), 283–301, 1962.

Allan, R.R., Cook, G.E. The long-period motion of the plane of a distant circular orbit. Proc. R. Soc. Lond. A 280, 97–109, 1964.

Allan, R.R., Cook, G.E. Discussion of paper by S.J. Peale, 'Dust Belt of the Earth'. J. Geophys. Res. 72, 1124–1127, 1967.

Anselmo, L., Pardini, C. Long-term dynamical evolution of high area-to-mass ratio debris released into high earth Orbits. Acta Astronaut. 67, 204–216, 2010.

Battin, R.H. An Introduction to the Mathematics and Methods of Astrodynamics, Revised Edition. American Institute of Aeronautics and Astronautics, 1999.

Bogoliubov, N.N., Mitropolski, Y.A. Asymptotic Methods in the Theory of Non-Linear Oscillations. Gordon and Breach, 1961.

Chao, C.C. Analytical Investigation of GEO Debris with High Area-to-Mass Ratio. In: Presented at the AIAA/AAS Astrodynamics Specialist Conference, Keystone, Colorado, Paper AIAA-2006-6514, 2006.

Folkner, W. M., Williams, J. G., Boggs, D. H. The planetary and Lunar ephemeris DE 421. The Interplanetary Network Progress Report, pp. 42–178, 2009.

Hubaux, Ch., Libert, A.-S., Delsate, N., Carletti, T. Influence of Earth's shadowing effects on space debris stability. Adv. Space Res. 51, 25–38, 2013.

Kyrloff, N., Bogoliuboff, N. Introduction to Non-Linear Mechanics. Princeton University Press, 1947.

Lemaître, A., Delsate, N., Valk, S. A web of secondary resonances for large A/m geostationary debris. Celest. Mech. Dyn. Astron. 104, 383–402, 2009.

Lidov, M.L. The evolution of orbits of artificial satellites of planets under the action of gravitational perturbations of external bodies. Planet. Space Sci. 9, 719–759, 1962.

Liou, J.-C., Weaver, J.K. Orbital dynamics of high area-to-mass ratio debris and their distribution in the geosynchronous region. In: Proceedings of the Fourth European Conference on Space Debris, Darmstadt, Germany, Paper ESA SP-587, 2005.

Mignard, F., Hénon, M. About an unsuspected integrable problem. Celest. Mech. Dyn. Astron. 33, 239–250, 1984.

Milankovitch, M., Kanon der Erdbestrahlung und seine Anwendung auf das Eiszeitenproblem. Königlich Serbische Akademie, 1941. (Canon of Insolation and the Ice-age Problem, English translation by Israel Program for Scientific Translations, 1969).

Musen, P. The influence of the solar radiation pressure on the motion of an artificial satellite. J. Geophys. Res. 65 (5), 1391–1396, 1960.

Musen, P. On the long-period Lunar and Solar effects on the motion of an artificial satellite, 2. J. Geophys. Res. 66 (9), 2797–2805, 1961.

Perozzi, E., Roy, A.E., Steves, B.A., Valsecchi, G.B. Significant high number of commensurabilities in the main Lunar problem. I: The Saros as a near-periodicity of the Moon's orbit. Celest. Mech. Dyn. Astron. 52, 241–261, 1991.

Richter, K., Keller, H.U. On the stability of dust particle orbits around cometary nuclei. Icarus 114, 355–371, 1995.

Rosengren, A., Scheeres, D. Averaged dynamics of HAMR Objects: effects of attitude and Earth oblateness. In: Presented at the AAS/AIAA Astrodynamics Specialist Conference, Girdwood, Alaska, Paper AAS 11–594, 2011.

Rosengren, A., Scheeres, D. Long-term dynamics of HAMR objects in HEO. In: Presented at the AIAA/AAS Astrodynamics Specialist Conference, Minneapolis, Minnesota, Paper AIAA 2012–4745, 2012.

Rosengren, A.J., Scheeres, D.J. On the milankovitch orbital elements for perturbed Keplerian motion. Celest. Mech. Dyn. Astron., submitted for publication.

Roy, A.E. Orbital Motion, fouthth ed Taylor & Francis, 2005.

Sanders, J.A., Verhulst, F., Murdock, J. Averaging Methods in Nonlinear Dynamical Systems, second ed Springer, 2007.

Scheeres, D.J. Orbital Motion in Strongly Perturbed Environments: Applications to Asteroid Comet and Planetary Satellite Orbiters. Springer–Praxis, 2012a.

Scheeres, D.J. Orbit mechanics about asteroids and comets. AIAA J. Guid. Cont. Dyn. 35 (3), 987–997, 2012b.

Scheeres, D., Rosengren, A., McMahon, J. The dynamics of high area-to-mass ratio objects in Earth orbit: The Effect of Solar Radiation Pressure. Presented at the AAS/AIAA Space Flight Mechanics Meeting, New Orleans, Louisiana, Paper AAS 11–178, 2011.

Schildknecht, T. Optical surveys for space debris. Astron. Astrophys. Rev. 14, 41–111, 2007.

Schildknecht, T., Musci, R., Ploner, M., Beutler, G., Flury, W., Kuusela, J., de Leon Cruz, J., de Fatima Domingueq Palmero, L. Optical observations of space debris in GEO and in highly-eccentric orbits. Adv. Space Res. 34, 901–911, 2004.

Struble, R.A. An application of the method of averaging in the theory of satellite motion. J. Math. Mech. 10, 691–704, 1961.

Tamayo, D., Burns, J.A., Hamilton, D.P., Nicholson, P.D. Dynamical instabilities in high-obliquity systems. Astron. J. 145, 54–65, 2013.

Tremaine, S., Touma, J., Namouni, F. Satellite dynamics on the Laplace surface. Astron. J. 137, 3706–3717, 2009.

Valk, S., Lemaître, A., Anselmo, L. Analytical and semi-analytical investigations of geosynchronous space debris with high area-to-mass ratios. Adv. Space Res. 41, 1077–1090, 2008.